



## Nanocellulose aerogel inserts for quantitative lateral flow immunoassays

Ye Tang<sup>a,b</sup>, Hui Gao<sup>a</sup>, Felix Kurth<sup>a</sup>, Loïc Burr<sup>a</sup>, Konstantinos Petropoulos<sup>a</sup>, Davide Migliorelli<sup>a</sup>, Olivier T. Guenat<sup>b</sup>, Silvia Generelli<sup>a,\*</sup>

<sup>a</sup> Swiss Center for Electronics and Microtechnology CSEM, Landquart Regional Center, Bahnhofstrasse 1, 7302, Landquart, Switzerland

<sup>b</sup> University of Bern, ARTORG Center for Biomedical Engineering Research, Organs-on-Chip Technologies, Murtenstrasse 50, 3008, Bern, Switzerland

### ARTICLE INFO

#### Keywords:

Lateral flow immunoassay  
Nanocellulose aerogel  
Quantitative point-of-care diagnostics  
Extended sample flow time

### ABSTRACT

The Lateral Flow Immuno Assay (LFIA) is a well-established technique that provides immediate results without high-cost laboratory equipment and technical skills from the users. However, conventional colorimetric LFIA strips suffer from high limits of detection, mainly due to the analysis of a limited sample volume, short reaction time between the target analyte and the conjugation molecules, and a weak optical signal. Thus, LFIAs are mainly employed as a medical diagnostic tool for qualitative and semi/quantitative detection, respectively. We applied a novel cellulose nanofiber (CNF) aerogel material incorporated into LFIA strips to increase the sample flow time, which in turn extends the binding interactions between the analyte of interest and the detection antibody, thus improving the limit of detection (LOD). Compared to a conventional LFIA strip, the longer sample flow time in the aerogel modified LFIA strips improved the LOD for the detection of mouse IgG in a buffer solution by a 1000-fold. The accomplished LOD (0.01 ng/mL) even outperformed specifications of a commercial ELISA kit by a factor of 10, and the CNF aerogel assisted LFIA was successfully applied to detect IgG in human serum with a LOD of 0.72 ng/mL. Next to the improved LOD, the aerogel assisted LFIA could quantify IgG samples in buffer and human serum in the concentration ranges of 0.17 ng/mL - 100 ng/mL (in buffer) and 4.6 ng/mL - 100 ng/mL (in human serum). The presented solution thus poses a unique potential to transform lateral flow assays into highly sensitive, fully quantitative point-of-care diagnostics.

### 1. Introduction

Lateral flow immunoassays (LFIA) are simple-to-use, rapid, low-cost, and portable, and have become an increasingly important Point-of-Care (POC) device in medical diagnostics and home testing (Mahmoudi et al., 2019; Mohd Hanafiah et al., 2017). Current LFIA applications span a plethora of clinically relevant biomarkers in a variety of biological samples, such as human chorionic gonadotropin (hCG) in urine for pregnancy tests (Butler et al., 2001), cardiac-specific troponins I and T in whole blood or plasma for heart attack detection (Cai et al., 2018), cortisol detection in sweat (Dalirirad and Steckl, 2019), and periodontal disease detection in saliva (Johnson et al., 2016). LFIAs furthermore play a significant role in the detection of infectious diseases. For instance, in relation to the current COVID pandemic, LFIAs are developed to enable fast and qualitative detection of immunoglobulin M (IgM) and immunoglobulin G (IgG) antibodies (Broughton et al., 2020; Li et al., 2020; Wu et al., 2020), antigens (Grant et al., 2020) and RNA (Wang et al., 2020) in suspects specifically in response to a SARS-COV-2

infection. The main drawback of this POC diagnostic tool is its low sensitivity (i.e., the limit of detection, LOD, at a high concentration) for the test of clinical biomarkers of interest. As a consequence, LFIAs are currently only employed for qualitative and semi/quantitative detection (Kasetsirikul et al., 2020; Tang et al., 2020). Thus, there is a significant demand to develop more sensitive LFIAs with lower LODs, reducing the number of false negative test results when detecting disease biomarkers that can be present at low abundance. Previous work improving lateral flow strip LODs focused primarily on two aspects: the immunoassay components and the lateral flow strip design. Improvements of the immunoassay aimed at introducing new label-detection antibody conjugates instead of conventional gold nanoparticle (AuNP)-detection antibody conjugates to enhance the signal output on the test line. For example, enzymes (Cho and Irudayaraj, 2013), quantum dots (Qu et al., 2016), carbon nanotubes (Qiu et al., 2015), magnetic nanoparticles (Moyano et al., 2020), fluorescent nanoparticles (Gong et al., 2017), liposomes (Edwards et al., 2017), and nanoparticles made of other metals or composited metals (Anfossi et al., 2019; Tian et al., 2019) have

\* Corresponding author.

E-mail address: [silvia.generelli@csem.ch](mailto:silvia.generelli@csem.ch) (S. Generelli).

<https://doi.org/10.1016/j.bios.2021.113491>

Received 17 February 2021; Received in revised form 31 May 2021; Accepted 6 July 2021

Available online 9 July 2021

0956-5663/© 2021 Published by Elsevier B.V.

been applied recently for the enhancement of the signal intensity on the test lines, thereby allowing for the detection of lower target analyte concentrations. The other proposed strategy for improving LFIA sensitivity is the modification of the lateral flow strip design with the primary goal to prolong the sample flow time – that is to say – the time a dispensed sample needs to pass the strip until it reaches the test and control lines. An increased sample flow time leads to a longer reaction time between detection antibodies and target analytes, which improves the binding efficiency between them, and ultimately enhances the sensitivity of LFIAs (Katis et al., 2018; Parolo et al., 2013). Concepts that have demonstrated different extends of increased sample flow times by lateral flow strip re-design comprise the use of a longer strip, new shapes of the sample and the conjugate pads (Fu et al., 2011; Choi et al., 2017), or the introduction of printed wax or PDMS pillars on the nitrocellulose pad (Rivas et al., 2014; Choi et al., 2016). In this work, we present a novel strategy to decrease the LOD of LFIAs as well as to render a quantitative analysis possible. We incorporated a cellulose nanofiber (CNF) aerogel in between the conjugate pad and the nitrocellulose strip of a conventional lateral flow device to extend the sample flow time (Fig. 1). CNF aerogel is an extremely good candidate as a stacking pad in a LFIA strip because it is characterized by a foam-like, porous structure that upon liquid wetting transforms into a transition state with hydrogel-like properties (Sun et al., 2019). We selected 2,2,6,6-tetramethylpiperidyl-1-oxyl (TEMPO)-oxidized cellulose nanofibers (CNF) to fabricate the CNF aerogel as the TEMPO-CNF exhibits high elastic moduli, high strengths, high thermal stability, large surface areas, and high aspect ratios that altogether help to produce a mechanically stable nanocellulose aerogel (Jiang and Hsieh, 2014). Compared to former

work following a similar strategy (Tang et al., 2017), the CNF aerogel is made from nanoscale cellulose materials. It is part of the same material class as all other lateral flow strip components. These cellulose-based materials exhibit intrinsically good wicking action and hydrophilic properties (Costa et al., 2014; Gasperino et al., 2018; Ng et al., 2017). Unlike other flexible, porous material candidates to be used as stacking pads with microscale pore sizes, the wetted transition state of the CNF aerogel is expected to have pore sizes of about 100 nm (Zander et al., 2014; Al-Sabah et al., 2019), thereby providing sufficient capillary forces for sample transport. One of the most advantageous properties of the CNF aerogel is, however, that due to its material properties, no additional surface functionalization and pretreatment of the CNF aerogel is required, which allows keeping fabrication simple and pricing low.

We examined the potential of the CNF aerogel-assisted lateral flow strip to improve the LOD of a LFIA targeting mouse IgG as a model system. Target analyte detection was investigated in buffer solution as well as in human serum, and the aerogel assisted LFIA performance compared to a conventional lateral flow strip design (no CNF-aerogel, cf. Fig. 1A and B).

## 2. Materials and methods

### 2.1. Chemicals and lateral flow strip components

2,2,6,6-tetramethylpiperidine-1-oxyl-cellulose nanofibers (TEMPO-CNF; carboxyl content: 0.2 mmol/g - 2 mmol/g, the University of Maine, ME, USA), 18 nm colloidal gold affini pure goat anti-mouse IgG (H + L; AuNP-anti-mouse IgG), affini pure rabbit anti-goat IgG (H + L), and

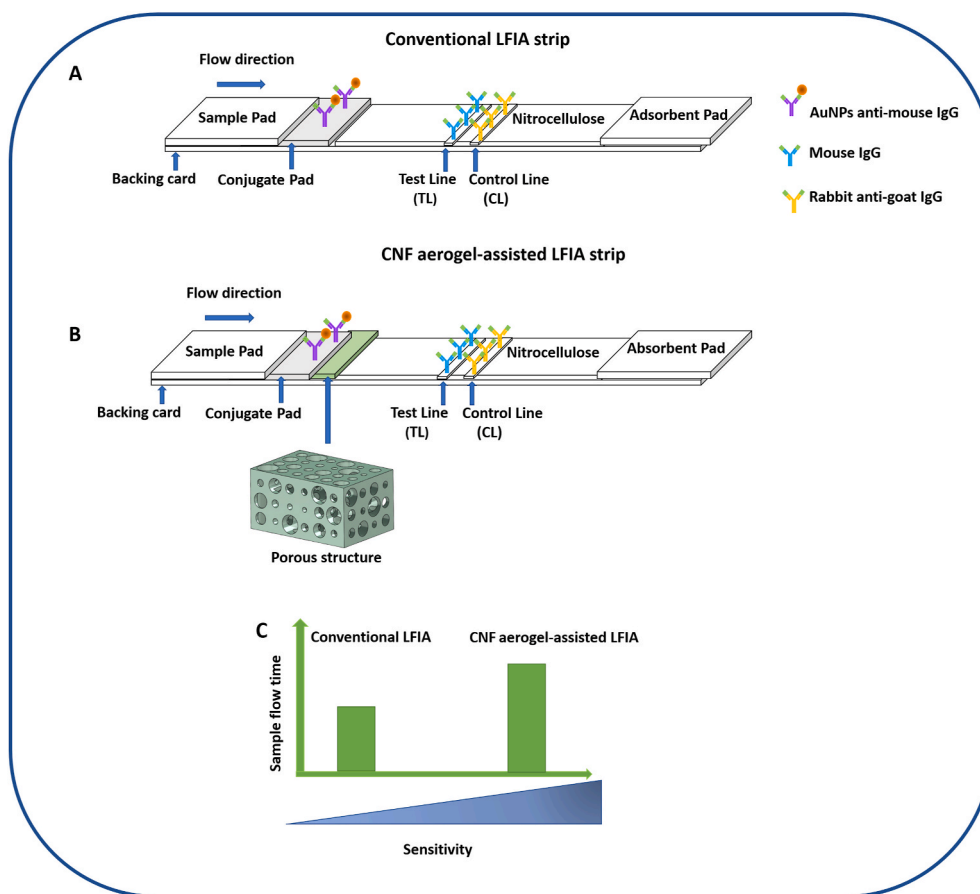


**Fig. 1.** Schematic comparison between a conventional LFIA strip design (A) and the CNF aerogel-assisted LFIA strip design (B). The CNF aerogel is integrated between the conjugate pad and the nitrocellulose membrane. (C) The integration of the CNF aerogel leads to an extended sample flow time and, hence, a more efficient binding between the target analyte and the detection antibody, which results in a higher assay sensitivity (detection of much lower target analyte concentrations).

ChromPure mouse IgG (whole molecule) were purchased from Jackson Immuno Research (Cambridgeshire, UK). Calcium chloride (>93%), phosphate buffered saline (PBS), albumin from bovine serum (BSA; >98%), Tween 20, human serum (from human male plasma, USA origin, sterile-filtered, H4522), 1, 2, 3, 4-butane tetracarboxylic acid (BTCA, 99%), rosa bengal dye (content 95%), and sodium hypophosphite (SHP, 99%) were purchased by Sigma-Aldrich (Buchs, Switzerland). Deionized water was produced by a Merck Milli-Q water purification system. Sample pad and adsorbent pad (C083 Cellulose Fiber Strips) were bought from Merck Millipore (Darmstadt, Germany). Glass fiber conjugate pad sheets (GFCP203000) and FFHP Plus nitrocellulose membranes (10547040, 400 nm pore diameter) were obtained from GE Health Care Europe GmbH (Freiburg, Germany), and backing pad (80 mm) was obtained from DCNOVATIONS (Carlsbad, CA USA).

## 2.2. Fabrication and characterization of different CNF aerogels

CNF aerogels were prepared using 2,2,6,6-tetramethylpiperidine-1-oxyl-cellulose nanofibers (TEMPO-CNF). In brief, CNF aerogels were fabricated in three steps as described before (Saito et al., 2007): (i) dispersing cellulose nanofibers in water with ultrasonic or mechanical treatment, (ii) forming CNF gels via a sol-gel process (iii) followed by lyophilization. Since the LFIA measurement will undergo a wetting state, we fabricated different sorts of CNF-based aerogels to identify the CNF aerogel with the best stability under wet conditions.

### 2.2.1. CNF aerogel without cross-linking

CNF aerogel without cross-linking was prepared as the following: 2 g of TEMPO-CNF powder were added into 200 mL of Milli-Q water to obtain a 1 wt% CNF suspension. The suspension was vigorously stirred (2000 rpm; IKA RW 20 stirrer, IKA, Staufen, Germany) at room temperature (RT) for 30 min until the suspension became homogeneous. Via mechanical stirring, the nanocellulose fibers in suspension formed the physical entanglement to yield a hydrogel. Subsequently, the hydrogel was added into a 6-well plate (2.5 mL of hydrogel per well) and kept at RT for 30 min to eliminate air bubbles. The 6-well plate containing the hydrogels was then transferred to a refrigerator and frozen at  $-20\text{ }^{\circ}\text{C}$  for 5 h. The frozen hydrogels were transferred into a lyophilizer (model alpha 1-4, Christ Gefriertrocknungsanlagen GmbH, Osterode am Harz, Germany) and freeze-dried at  $-55\text{ }^{\circ}\text{C}$  for 24 h. The obtained aerogel was stored under ambient conditions at RT until use.

### 2.2.2. CNF aerogel with physical cross-linking

The CNF aerogel with physical cross-linking was prepared via the ionic interactions between the negative charge of TEMPO-CNF and  $\text{Ca}^{2+}$  (Basu et al., 2017) (Fig. S1). Five grams of  $\text{CaCl}_2$  (2.5 wt%) were added into 200 mL of 1 wt% TEMPO-CNF suspension, which was prepared using the protocol described above. The physical cross-linking between CNF fibers in suspension was formed under stirring using a magnetic stirrer for 12 h at RT. The physically cross-linked hydrogel was freeze-dried following the identical procedure described above, and the resulting aerogel was stored likewise.

### 2.2.3. CNF aerogel with chemical cross-linking

The CNF aerogel with chemical cross-linking was synthesized via an esterification reaction between the carboxylic acid groups of 1, 2, 3, 4-butane tetracarboxylic acid (BTCA) and the hydroxyl groups of TEMPO-CNF. Sodium hypophosphite (SHP) was added as a catalyst for the reaction (Chen et al., 2019) (Fig.S2). BTCA (200 mg; 10 wt% of TEMPO-CNF powder) and SHP (20 mg; 10 wt% of BTCA) were added into 200 mL of 1 wt% TEMPO-CNF suspension and the reaction mixture was stirred for 12 h at RT to complete the formation of chemically cross-linked CNF hydrogel. Lyophilization and subsequent storage of the product were conducted the same as described above.

## 2.3. Stability test of CNF aerogel in aqueous solution

Since liquid samples pass the aerogel as part of the lateral flow assay, the aerogels must be stable in solution. The fabricated CNF aerogels (no cross-linking, with physical or chemical cross-linking) were thus tested for their stability in a buffer solution. The aerogels were diced into small pieces ( $1\text{ cm}^2$ ) and immersed in 2 mL buffer solution (PBS buffer containing 0.05% Tween 20 and 1% BSA) at RT. The structural stability of the different CNF aerogels was observed and compared at the following different time points after immersion: 5 min, 10 min, and 2 h.

## 2.4. Morphology characterization of the chemically cross-linked nanocellulose aerogel

Scanning electron microscopy (SEM) images of the chemically-crosslinked CNF aerogel were acquired using a Hitachi S-3400N scanning electron microscope at accelerating voltages of 20 kV and working distances of 17 mm. Before the measurement, the samples were coated with a layer of gold (about 5 nm) using a Cressington 108 auto automatic sputter coater. Sample preparation and SEM imaging of CNF aerogels taken from used lateral flow strips after running the LFIA followed the same procedure (Fig.S3).

## 2.5. Immunoassay description and data readout

The potential of using the CNF aerogel-assisted LFIA for decreasing the limit of detection was investigated by quantifying mouse IgG spiked in buffer and in human serum. A competitive IgG-anti-IgG immunoassay was chosen and tested with LIFAs with and without CNF aerogels. Different concentrations of mouse IgG were spiked into a running buffer (PBS buffer containing 0.05% Tween 20 and 1% BSA) and added onto the sample pad (total volume added: 100  $\mu\text{L}$ ). The sample was transported towards the conjugate pad by capillary forces, onto which the detection antibody (AuNP-anti-mouse-IgG) had been immobilized. During the transport towards the test and control lines, the mouse IgG bound to the AuNPs-anti-mouse IgG to form the mouse IgG-AuNP-anti-mouse-IgG complex. The unbound AuNP-anti-mouse IgG is captured by the immobilized mouse IgG on the test line, while the formed mouse IgG-AuNP-anti-mouse IgG complex continues to flow through the nitrocellulose until it is captured by the rabbit-anti-goat IgG immobilized on the control line. The color intensity on each line displays the amount of the captured gold nanoparticles, i.e. either the IgG-AuNP-anti-mouse-IgG complex or the pure AuNP-anti-mouse-IgG. Since the immunoassay represents a competitive assay design, this color intensity decreased on the test line with increasing IgG sample concentrations. Sample fluid that already passed the nitrocellulose strip was collected by the absorbent pad.

Thirty minutes after sample application, the color intensities of the test and control lines were correlated to the sample mouse IgG concentration as the following: pictures of the test and control lines were taken at a distance of 5 cm using a Huawei mate 20 pro cell phone (Fig. S4 A). The gray values of test and control lines were extracted by Image J (32-bit grayscale mode), and the ratio of the gray values (R; gray value test line over gray value control line) was calculated ( $R = 100 \times T/C$ ,  $T =$  gray value of the test line,  $C =$  gray value of the control line) (Fig. S4 B). A strong line color (high AuNP amount, dark) results in a low gray value and a faint line color (low AuNP amount, bright) results in a high gray value ratio (see also explanations given in Fig. S4C). The gray value ratios were plotted against the mouse IgG sample concentrations to obtain a calibration curve. Data analysis was conducted with unmodified images, whereas pictures of the LFIA strips used for illustrative purposes in figures were adapted in contrast and brightness for better visibility. Small inconsistencies in the line intensities in the figure images may originate from these adaptations.

## 2.6. Fabrication of the lateral flow strips with and without CNF aerogel

LFIA strips were fabricated with and without the integration of CNF aerogel stacks. The standard LFIA consists of a cellulose-based sample pad, a glass fiber-based conjugation pad, a nitrocellulose membrane, and a cellulose-based adsorbent pad (Fig. 1). The final 5 mm-wide lateral flow strips were prepared by assembling one lateral flow strip (10 cm width) that was cut into narrower, individual lateral flow strips (5 mm) after final assembly. Mouse IgG (1.0 mg/mL in PBS) and rabbit anti-goat IgG (0.9 mg/mL in PBS) solutions were dispensed on the nitrocellulose membrane (30 mm × 10 cm, length × width) using a Biodot XYZ3060 platform (Printing speed: 50 mm/s, printing rate: 0.4 μL/cm, drop volume: 4.0 nL; Biodot, London, England) to form the test line and the control line, respectively. The position of the test line was printed with a distance of 15 mm to the conjugate pad, and the control line was printed an additional 15 mm away from the conjugate pad. After dispensing the test and control lines, the nitrocellulose membrane was dried at 37 °C in a vacuum chamber for 2 h. The conjugate pad was prepared by pipetting a defined volume (see chapter “Conjugate pad optimization” for details) of AuNP-anti-mouse IgG solutions onto a glass fiber pad (8 mm × 10 cm, length × width). The functionalized conjugate pad was dried under ambient conditions overnight and stored at 4 °C until use. The sample pad (15 mm × 10 cm, length × width) and the adsorbent pad (20 mm × 10 cm, length × width) were used as received from the supplier without any further pretreatment. All prepared LFIA parts were assembled on a polyester-based plastic adhesive backing pad with a 2 mm overlap between each adjacent stack to ensure sample flow through the entire strip. Finally, the prepared LFIA pad was cut manually into 5 mm wide strips.

The CNF aerogel-assisted LFIA strips contain an extra piece of CNF aerogel (3 mm–5 mm of length × 10 cm width) between the conjugate pad and the nitrocellulose pad. Three lengths (3 mm, 4 mm, and 5 mm) were tested (Fig. S5) and assembled in 10 cm wide pads into the final strip design. Both types of fabricated LFIA strips were stored in vacuum packaging at 4 °C until use.

### 2.6.1. Conjugate pad optimization

The amount of dispensed detection antibodies (AuNP-anti-mouse IgG) on the conjugate pad is a crucial factor affecting the detection limit of the LFIA. The optimal amount of detection antibody was identified by dispensing three different volumes (1 μL, 2 μL, 3 μL) of AuNP-anti-mouse IgG solution (0.5 mL supplied stock solution already containing 0.01 M sodium borate – sodium phosphate, 0.15 M NaCl, and 15 mg/mL BSA) onto the conjugate pad. After final lateral flow strip assembly including the 4 mm long CNF aerogel, the three different LFIA versions were characterized by analyzing three different mouse IgG concentrations (0 ng/mL, 1 ng/mL, 100 ng/mL) in running buffer. The optimal amount of detection antibody solution was supposed to provide increasing gray value ratios (intensity test line over intensity control line) with increasing concentrations of mouse IgG in the sample. All concentrations were measured in triplicates for each LFIA-conjugate pad version (data is shown in Fig. S6).

### 2.6.2. LFIA reproducibility test

We evaluated the reproducibility of the different types of LFIA strips by calculating the relative standard deviations (RSD) of the gray value ratios from 6 different strips after running a blank sample, i.e., running buffer without mouse IgG. RSD values were calculated according to  $RSD = (SD/average) * 100\%$ , whereby SD is the standard deviation and average is the mean value of the 6 different gray value ratios. Conventional LFIA strips and LFIA strips with a 4 mm long aerogel were tested. The RSD values are listed in Table S1.

## 2.7. Modulation of the sample flow time using integrated CNF aerogels

LFIA strips were prepared with the integration of nanocellulose

aerogels of 0.5 mm thickness and different lengths (3 mm, 4 mm, 5 mm). A rosa bengal dye solution (100 μL at 1 g/L in ddH<sub>2</sub>O) was dispensed onto the sample pad, and the migration of the colored solution documented at different time points after dispensing (30 s, 60 s, 90 s, 120 s, 150 s, 180 s, 210 s, 240 s, 270 s, 300 s). The respective fluid flow speeds were determined by linear fits of the liquid propagation within the time period of constant fluid migration (Fig. S7).

## 3. Results and discussion

### 3.1. Fabrication and characterization of nanocellulose aerogels

#### 3.1.1. Wet stability test of CNF aerogels in aqueous solution

We fabricated three sorts of CNF aerogel: an aerogel without fiber cross-linking, with physical cross-linking, and with chemical cross-linking (Fig. 2A). Since the LFIA strip incorporated CNF aerogel will undergo wetting by the sample, we tested the three CNF aerogel types in aqueous solution for their stability (Fig. 2B). Given an estimated average operational time of the LFIA sensor of up to 30 min, we aimed at maintaining its physical stability for at least that amount of time. The CNF aerogels without cross-linking showed poor structural stability with complete disintegration after 10 min. This can be reasoned by the aerogel network structure, which is built by hydrogen bonds and physical entanglements between adjacent CNFs. Upon exposure to the buffer solution, the cellulose-water hydrogen bonds replace the inter-fiber hydrogen bonds, consequently disintegrating the aerogel network structure. The aerogels formed by physical cross-linking treatment also underwent disintegration after placing them in buffer solution (starting after 5 min). Hereby, the diffusion of the Ca<sup>2+</sup> from the aerogel into the solution destroyed the cross-linking aerogel structure. It was furthermore observed that the formed Ca<sup>2+</sup> based salts precipitated within the phosphate buffer hosting solution. In contrast, the structural stability of CNF aerogel was improved by chemical cross-linking. It is based on the esterification reaction between the hydroxylic group of CNF and carboxylic groups of 1, 2, 3, 4 butane tetracarboxylic acid (BTCA). As a result (Fig. 2B right), the chemically cross-linked CNF aerogel maintained its original structure in buffer solution for more than 2 h. Since the chemically cross-linked CNF aerogel proved to stay stable in aqueous solution, further characterization and integration into LFIA strips continued using this aerogel construct only. It is to be noted that the chosen CNF aerogel was also employed for tests in human serum diluted at a 1:1 ratio with buffer solution (cf. Fig. 6), where it also did not show any indications for material deterioration. We also started employing the material for tests in human saliva, where material behavior proved likewise (data not shown). Further shelf-life tests proved the stability of 6 months at least, and since the aerogel is integrated into the strip in its dry state as a separate building block, we do not anticipate any deviation from the tests performed with the CNF aerogel alone as well as do not expect the aerogel to affect the shelf-life of the LFIA strip itself.

#### 3.1.2. Morphology characterization of the chemically cross-linked nanocellulose aerogel

Scanning electron microscopy (SEM) was used to analyze the morphology of the chemically cross-linked CNF aerogel. Sample preparation consisted of hydrogel formation in buffer followed by freeze-drying, during which formed ice crystals were sublimated, thereby conserving the voids within the microporous structure (Lavoine and Bergström, 2017). Fig. 3A and B shows that the chemically cross-linked CNF aerogel exhibits very thin solid sheets and an interconnected porous structure with pore sizes up to 200 μm. Pore sizes of these dimensions may be disadvantageous for effective sample flow reduction in a lateral flow strip. But as already pointed out, the aerogel transforms into a hydrogel-like state upon wetting (Sun et al., 2019). During absorption of the sample solution, the pore sizes decrease to about 100 nm (Zander et al., 2014; Al-Sabah et al., 2019). The hydrophilic surface properties of the CNF material enable the solution to be transported by capillary

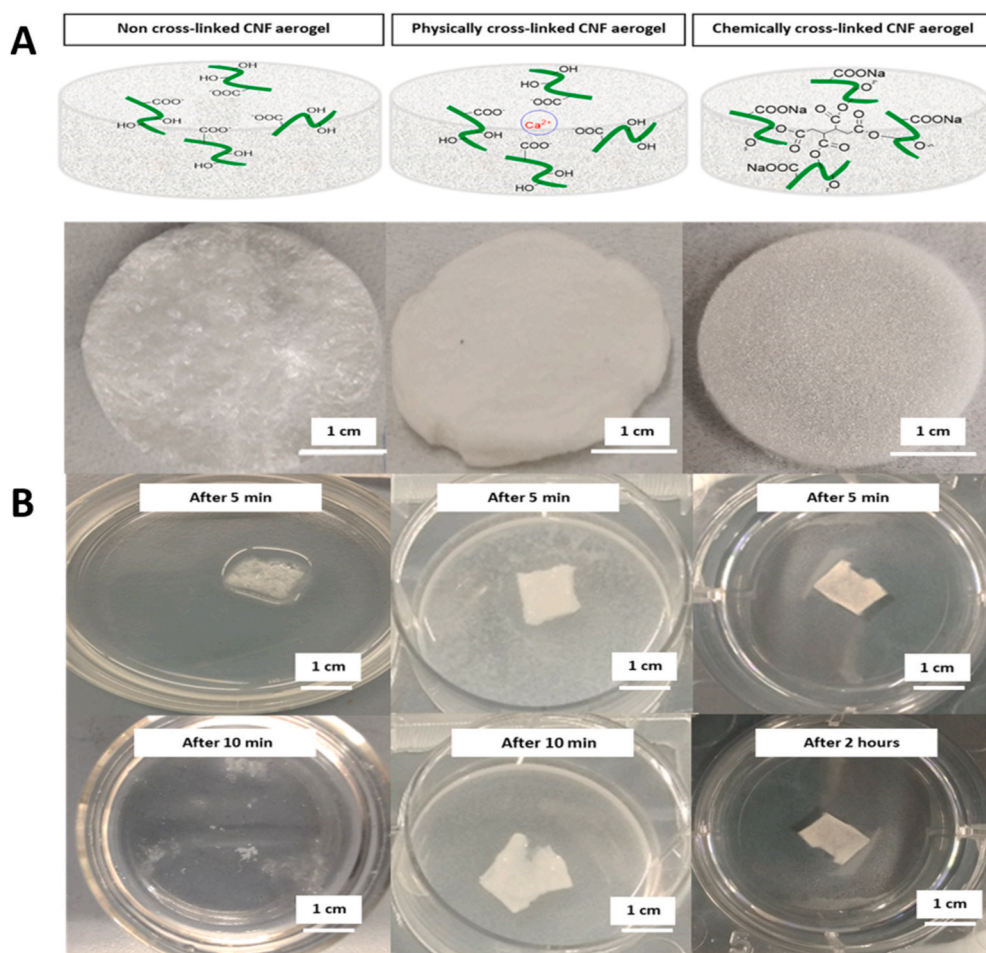


**Fig. 2.** Wet stability test of CNF aerogel without crosslinking (left), with physical crosslinking (middle), and with chemical crosslinking (right). (A) The pictures of the different aerogels depict their morphologies in a dry state. (B) Pictures of the three different CNF aerogels, each at the size of 1 cm<sup>2</sup>, after immersion in buffer solution: the CNF aerogel without crosslinking was stable for 5 min but disintegrated completely 5 min later; the physically cross-linked aerogel immediately caused the precipitation of Ca<sup>2+</sup> based salts and started to disintegrate after 10 min. In contrast, the chemically cross-linked CNF aerogel kept its original structure in buffer solution after 2 h of immersion in buffer solution.

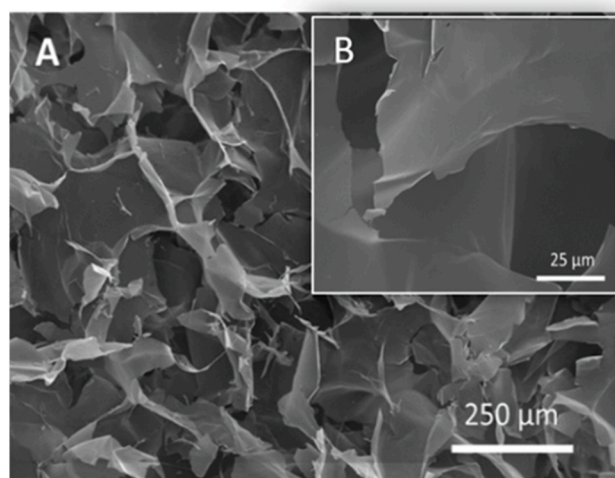


**Fig. 3.** SEM images of chemically cross-linked CNF cellulose aerogels in dry state at two magnifications. The pore sizes are very heterogeneous and range up to approximately 200 μm (A, B).

forces in the porous material.

### 3.2. Modulation of the sample flow time using integrated CNF aerogels

In order to increase the reaction time between the analyte of interest and the detection antibodies, the sample flow time needs to be increased

accordingly. To this end, we incorporated different lengths of the aerogel implemented into the LFIA strips and compared the resulting sample flow times with the one of a conventional LFIA strip. We stacked 0.5 mm thick aerogels in two different lengths of 3 mm and 4 mm in between the conjugate pad and the nitrocellulose strip, and monitored the sample flow time of a hydrophilic red dye (rosa bengal) through the CNF aerogel-assisted and conventional LFIA strips (Fig. 4A–C). Thicker aerogel pads lead to the disintegration of the strip assembly during use (data not shown), and aerogels longer than 4 mm lead to partial disruption of the aerogel-nitrocellulose contact as shown in figure S5, both cases mainly occurring due to the geometry change of the aerogel during the wetting process. Fig. 4D depicts the sample flow times for all tested LFIA constructs shown in Fig. 4A–C. The results indicate that the sample flow time is increased by the incorporation of the aerogel, and that this increase is a function of the aerogel length. Compared to the LFIA strip without CNF aerogel, the integrated CNF aerogel caused a flow time of about 60 s and 90 s for aerogels of 3 mm and 4 mm length, respectively. This prolongs the reaction time between the target analytes and the detection antibodies by approximately 40%–60%.

The data in Fig. 4D exhibits different flow phases during the sample loading into and initial sample transport through the LFIA strips containing the aerogels. After an initial absorption of the sample by capillary forces that is almost identical to the LFIA strips without the aerogel (less than 30 s), the sample transport within the CNF aerogel-assisted LFIA strips stops for about 30 s. The interruption of the sample flow between 30 s and 60 s is due to the transition of the aerogel into the hydrogel-like state, absorbing water from the sample. After full wetting of the CNF aerogel, the sample is further transported through the strips at a slower rate compared to the conventional LFIA strip (cf. figure S7).

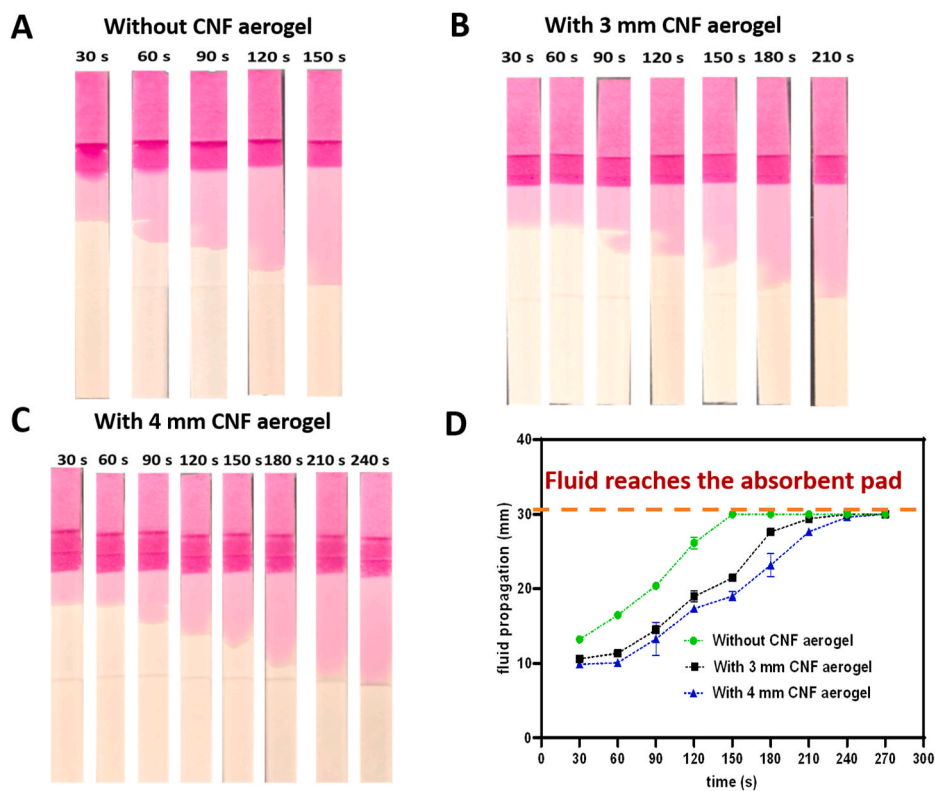


Fig. 4. Sample flow analysis within different LFIA constructs. Photographs were taken at different time points after liquid sample dispensing onto the sample pad (t = 30 s, 60 s, 90 s, 120 s, 150 s, 180 s, 210 s, 240 s, 270 s, and 300 s) to determine the time required for the sample to reach the absorbent pad. The total distance between the sample pad and the absorbent pad is 30 mm. Photographs represent the conventional LFIA (A), the CNF aerogel (3 mm length) modified LFIA (B), and the CNF aerogel (4 mm length) modified LFIA (C). All CNF aerogels were of 0.5 mm thickness. (D) Analyzed time-lapse sample flow in the three different LFIA constructs: data points represent mean values and standard deviations of three technical replicates per LFIA construct. The number in millimeters defines the CNF aerogel length.

The reduction of the flow rate is due to an increase of the hydraulic resistance of the flow path induced by the pores of the aerogel. This effect is further amplified with an increased length of the aerogel (Fig. 4D).

Since the 4 mm long aerogel provided the highest increase in sample flow time, we sought out to test this design as part of the IgG detection using the LFIA device.

### 3.3. Quantification of mouse IgG in buffer solution

In a first step, the amount of the pre-deposited AuNP-anti-mouse IgG was optimized to provide an increasing LFIA response – increasing color strength of the test line with increasing concentrations of mouse IgG in the sample – for mouse IgG spiked at different concentrations in buffer (0 ng/mL, 1 ng/mL, 100 ng/mL), cf. figure S7.

Next, conventional LFIA strips and aerogel-assisted (4 mm aerogel length) LFIA strips were both tested with 100 μL running buffer containing mouse IgG concentrations from as low as 0.01 ng/mL up to as

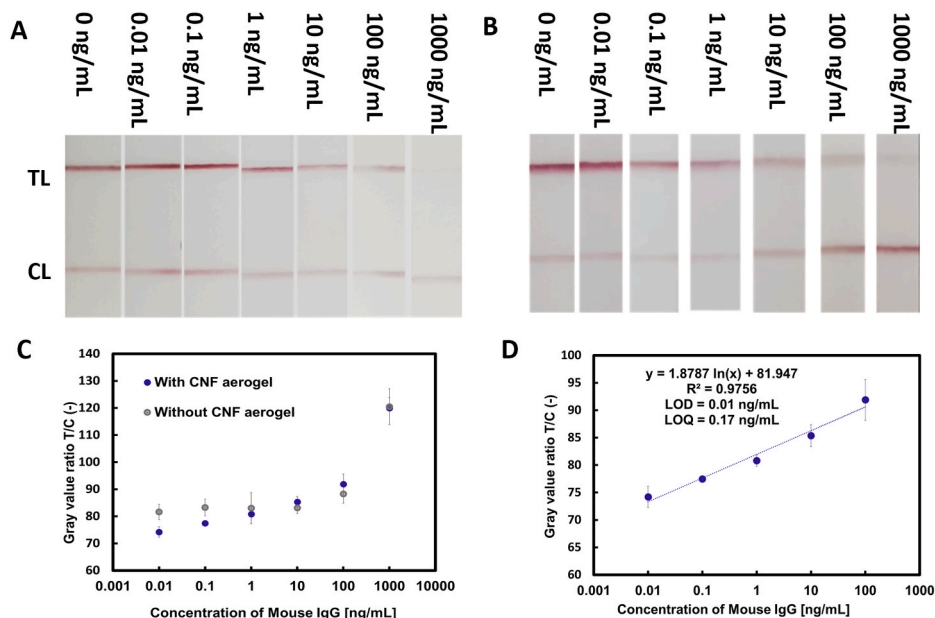


Fig. 5. Sensitivity analysis of the conventional and the CNF aerogel-assisted LFIAs. Different mouse IgG concentrations in buffer solution were tested (0 ng/mL–1000 ng/mL). (A) Photographs of conventional LFIA and (B) LFIA with CNF aerogel for samples containing 0.01–1000 ng/mL of mouse IgG. The color intensity of the test line decreases with increasing IgG concentrations for case B. The color intensity reflects the amount of bound gold nanoparticles on the respective line, and the gray value is lower for darker gray values (more color). (C) Comparison of the calibration curves of the LFIAs with (blue) and without (gray) CNF aerogel. The CNF aerogel-assisted LFIA allows for IgG detection as low as 0.01 ng/mL. In contrast, the conventional LFIA strip without aerogel can only qualitatively differentiate concentrations of >1 ng/mL from negative control results. (D) Fitting curve of the working range of the CNF aerogel-assisted LFIA for mouse IgG detection in buffer. The data in Fig. C and D represent mean values and standard deviations of n = 6 technical replicates for the conventional LFIA and CNF aerogel-assisted LFIA. TL: Test Line; CL: Control Line. (For interpretation of the references to color in this figure legend, the reader is referred to the Web version of this article.)

high as 1000 ng/mL (Fig. 5A and B), the strip results were analyzed for their test line over control line color intensity using pictures taken by a smartphone, and the mean gray value of selected area of test line and control line was measured directly by the ImageJ software (Figure S5). Then, the gray values of test and control lines were extracted by Image J (32-bit grayscale mode), and the ratio of the gray values (R; gray value test line over gray value control line) was calculated ( $R = 100 \times T/C$ , T = gray value of the test line, C = gray value of the control line) (Fig. 5C).

Whereby the conventional LFIA strips were only able to distinguish mouse IgG concentrations of 10 ng/mL and higher from negative control samples (no mouse IgG, for negative control values cf. table S1), the CNF aerogel-assisted LFIA strips allowed to lower this concentration by a factor of 1000, i.e., down to 0.01 ng/mL. Since the gray value ratios of the aerogel-assisted LFIA strip moreover continued to constantly increase with increasing mouse IgG concentrations up to 100 ng/mL, the introduced lateral flow strip design even showed its potential to quantify the analyte target in a wide concentration range (Fig. 5D). The limit of detection (LOD) and limit of quantification (LOQ) were calculated as  $3\text{ SD} + B$  (LOD) and  $10\text{ SD} + B$  (LOQ), whereby SD is the standard deviation of the blank sample, and B is the average value of the blank sample (Miller and Miller, 2010a; Brandon, 2011). The calculated LOD (0.01 ng/mL) and LOQ (0.017 ng/mL) values for the introduced new lateral flow strip concept are even comparable to specifications of a commercially-available ELISA kit (0.1 ng/mL – 500 ng/mL) (Mouse IgG ELISA development kit (ALP) 3825-1AD-6). Mouse IgG concentrations higher than 100 ng/mL could also be detected by the aerogel-assisted LFIA, however, only in a qualitative manner – same as the conventional LFIA.

In this study, we employ an immunoassay that is designed with an amount of AuNP-anti-mouse IgG that is not sufficient to saturate both test and control line in full. Although this can lead to a slight decrease in the control line signal upon a high amount of AuNP-anti-mouse IgG binding to the test line (cf. Fig. 5B, low IgG concentrations), the assay is designed in a way that even at a full saturation of the test line, the control line stays visible. Using this strategy, the calculated ratios of the test line by control line intensities are more sensitive to varying concentrations of IgG.

It is to be noted that although the aerogel undergoes a transition into a hydrogel-like state and, during this transition, absorbs water from the sample, we could not detect direct hints for irreversible sample absorption in the aerogel. Pictures taken after all applied fluid was successfully absorbed into the absorption pad (at least 1 h after sample application), thereby drying the rest of the lateral flow strip, could not document any red color originating from AuNPs (Fig. S3A). Both observations prove that the AuNP-anti-mouse IgG antibodies are not absorbed irreversibly by the aerogel, which in turn suggests no sample loss due to absorption in the aerogel. As a consequence, we thus also do not expect that the test and control line intensities are negatively affected by such absorption processes, which can potentially lead to false results.

Finally, the preparation of the test and control lines using automated

fluid dispensing resulted in slightly varying thicknesses of the printed lines although identical dispensing parameters were selected for each deposition on the same machine. This effect can be seen by directly comparing Fig. 5A and B. This thickness difference is most likely caused by the humidity difference during the printing process. The amount of the printed bioreagent is however identical for all printed batches used in this study. Since the test line and control line on the same strip were always affected likewise, the gray value ratio used for evaluation is effectively compensating for the printing variation.

#### 3.4. Quantification of mouse IgG in human serum

To evaluate the potential of the proposed method for the targeted clinical diagnostic application with a real biofluid, the CNF aerogel assisted LFIA strip was challenged with human serum (diluted at a volume ratio of 1:1 with running buffer) containing the identically spiked mouse IgG concentrations used for the tests in buffer (Fig. 6A and B). Compared to the results achieved in buffer solution, the working range was found to be congruent – that is to say – from 0.72 ng/mL up to 100 ng/mL. Higher mouse IgG concentrations were not tested in human serum. The determined LOD (0.72 ng/mL) and LOQ (4.6 ng/mL) values were calculated as in section 3.3 and were higher than those calculated for the test results obtained in buffer solution. This decrease in detection sensitivity in human serum is expected to be caused by matrix effects (Rosenberg-Hasson et al., 2014). Specifically, factors such as ionic strength, pH, cations, viscosity, and serum proteins, can decrease the binding efficiency between the detection antibody and the mouse IgG (Crisino et al., 2014). Besides, non-specific binding between the detection antibodies and interfering biological components, such as endogenous proteins (Sztefko, 2002) and existing antibody interferences (García-González et al., 2016; Levinson and Miller, 2002; Schwickart et al., 2014), supposedly renders the accurate measurement of the analyte of interest challenging. Further dilution of such complex samples with a buffer solution may help minimize the matrix effect in the future, as long as the sample IgG concentration does not fall below the LOQ for quantitative and below the LOD for qualitative analysis. Even though the measurement sensitivity of mouse IgG is slightly mitigated in human serum compared to the one in buffer solution, the developed CNF aerogel-assisted LFIA shows promising potential for quantitatively detecting biomarkers in patient samples.

#### 4. Conclusion

The novel approach improves the sensitivity of LFIA devices with the aim to lower the limit of detection and to facilitate quantitative analysis. We show that by integrating a CNF aerogel intermediate stack layer into a conventional LFIA device, the sample flow time is effectively increased and, as a consequence, an extended interaction time between the bioreagents results in up to a 1000-fold improvement of the limit of detection for mouse IgG. The modulated sample flow time and optimized detection analyte deposition additionally allowed for the

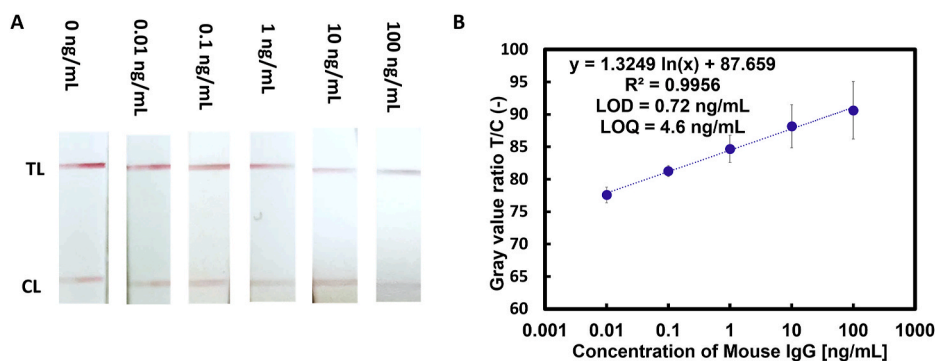


Fig. 6. Sensitivity analysis of the CNF aerogel modified LFIA for the test of mouse IgG in human serum. Different concentrations of mouse IgG were tested (0 ng/mL-1000 ng/mL). Same as for the tests in buffer, the color intensity of the test line decreases with increasing IgG concentrations. B) Fitting curve of the quantification range of the CNF aerogel assisted LFIA for mouse IgG detection in human serum. The data in chart B represent the mean values and the standard deviations of  $n = 6$  technical replicates for the CNF aerogel assisted LFIA. TL: Test Line; CL: Control Line. (For interpretation of the references to color in this figure legend, the reader is referred to the Web version of this article.)

quantification of a wide range of mouse IgG concentrations in a complex matrix. This underlines the potential of the novel strategy for lateral flow assays in clinical applications, which require improved detection limits to reduce false-negative test results. This is of high interest for applications aiming at monitoring disease progression and treatment for which quantitation is often inevitable. Since the same binding principles apply for other target analytes, we expect similar outcome for tests with other antibodies. The system may also be designed to monitor antigen detection. The first test results of CNF aerogel-assisted LFIA devices are indeed promising, however, their performance with more complex samples, for instance, full blood, still needs to be evaluated, and the analysis of clinical samples needs to be benchmarked with state-of-the-art procedures. Improvements in smartphone-based analysis will certainly help improving result interpretation and can at the same time be utilized for direct communication with professional healthcare channels. Due to its simplicity and cost-effectiveness, the proposed strategy can be easily extended to any type of LFIA design. As it exclusively affects the sample flow time and does not interfere with the assay itself, it is thus technically independent of the assay principle, which has been demonstrated as a general principle and in different assay formats (Katis et al., 2018; Tang et al., 2017). This technology thus bears a tremendous potential for lateral flow point-of-care devices in the clinics and for home testing.

### CRedit authorship contribution statement

**Ye Tang:** Conceptualization, Methodology, Data curation, Writing – original draft, preparation. **Hui Gao:** Conceptualization, Methodology, Supervision. **Felix Kurth:** Methodology, Data curation, Writing – review & editing. **Loïc Burr:** Methodology. **Konstantinos Petropoulos:** Methodology. **Davide Migliorelli:** Investigation. **Olivier T. Guenat:** Supervision. **Silvia Generelli:** Conceptualization, Supervision, Project administration.

### Declaration of competing interest

The authors declare that they have no known competing financial interests or personal relationships that could have appeared to influence the work reported in this paper.

### Acknowledgments

The authors acknowledge R. Junuzovic and L. Mühlebach for support in laboratory work, V. Zubkova for guidance in instrumental expertise, and S. Paoletti for fruitful discussions. The authors acknowledge H. Heinzelmann for the mentorship and financial support of the project.

### Appendix A. Supplementary data

Supplementary data to this article can be found online at <https://doi.org/10.1016/j.bios.2021.113491>.

### References

- Al-Sabab, A., Burnell, S.E.A., Simoes, I.N., Jessop, Z., Badiei, N., Blain, E., Whitaker, I.S., 2019. Structural and mechanical characterization of crosslinked and sterilised nanocellulose-based hydrogels for cartilage tissue engineering. *Carbohydr. Polym.* 212, 242–251. <https://doi.org/10.1016/j.carbpol.2019.02.057>.
- Anfossi, L., Di Nardo, F., Russo, A., Cavalera, S., Giovannoli, C., Spano, G., Baumgartner, S., Lauter, K., Baggiani, C., 2019. Silver and gold nanoparticles as multi-chromatic lateral flow assay probes for the detection of food allergens. *Anal. Bioanal. Chem.* 411, 1905–1913. <https://doi.org/10.1007/s00216-018-1451-6>.
- Basu, A., Hong, J., Ferraz, N., 2017. Hemocompatibility of Ca<sup>2+</sup>-crosslinked nanocellulose hydrogels: toward efficient management of hemostasis. *Macromol. Biosci.* 17, 1700236. <https://doi.org/10.1002/mabi.201700236>.
- Brandon, D.L., 2011. Detection of Ricin contamination in ground beef by electrochemiluminescence immunosorbent assay. *Toxins* 3, 398–408. <https://doi.org/10.3390/toxins3040398>.
- Broughton, J.P., Deng, X., Yu, G., Fasching, C.L., Singh, J., Streithorst, J., Granados, A., Sotomayor-Gonzalez, A., Zorn, K., Gopez, A., Hsu, E., Gu, W., Miller, S., Pan, C.-Y., Guevara, H., Wadford, D., Chen, J., Chiu, C.Y., 2020. Rapid detection of 2019 novel coronavirus SARS-CoV-2 using a CRISPR-based DETECTR lateral flow assay. *medRxiv*. <https://doi.org/10.1101/2020.03.06.20032334>, 2020.03.06.20032334.
- Butler, S.A., Khanlian, S.A., Cole, L.A., 2001. Detection of early pregnancy forms of human chorionic gonadotropin by home pregnancy test devices. *Clin. Chem.* 47, 2131–2136. <https://doi.org/10.1093/clinchem/47.12.2131>.
- Cai, Y., Kang, K., Li, Q., Wang, Y., He, X., 2018. Rapid and sensitive detection of cardiac troponin I for point-of-care tests based on red fluorescent microspheres. *Molecules* 23. <https://doi.org/10.3390/molecules23051102>.
- Chen, Y., Fan, D., Lyu, S., Li, G., Jiang, F., Wang, S., 2019. Elasticity-Enhanced and aligned structure nanocellulose foam-like aerogel assembled with cooperation of chemical art and gradient freezing. *ACS Sustain. Chem. Eng.* 7, 1381–1388. <https://doi.org/10.1021/acssuschemeng.8b05085>.
- Cho, I.H., Irudayaraj, J., 2013. Lateral-flow enzyme immunoconcentration for rapid detection of *Listeria monocytogenes*. *Anal. Bioanal. Chem.* 405, 3313–3319. <https://doi.org/10.1007/s00216-013-6742-3>.
- Choi, J.R., Liu, Z., Hu, J., Tang, R., Gong, Y., Feng, S., Ren, H., Wen, T., Yang, H., Qu, Z., Pingguan-Murphy, B., Xu, F., 2016. Polydimethylsiloxane-Paper hybrid lateral flow assay for highly sensitive point-of-care nucleic acid testing. *Anal. Chem.* 88, 6254–6264. <https://doi.org/10.1021/acs.analchem.6b00195>.
- Choi, J.R., Yong, K.W., Tang, R., Gong, Y., Wen, T., Yang, H., Li, A., Chia, Y.C., Pingguan-Murphy, B., Xu, F., 2017. Lateral flow assay based on paper-hydrogel hybrid material for sensitive point-of-care detection of dengue virus. *Adv. Healthc. Mater.* 6 <https://doi.org/10.1002/adhm.201600920>.
- Costa, M.N., Veigas, B., Jacob, J.M., Santos, D.S., Gomes, J., Baptista, P.V., Martins, R., Inácio, J., Fortunato, E., 2014. A low cost, safe, disposable, rapid and self-sustainable paper-based platform for diagnostic testing: lab-on-paper. *Nanotechnology* 25, 094006. <https://doi.org/10.1088/0957-4484/25/9/094006>.
- Crisino, R.M., Luo, L., Geist, B., Zoghbi, J., Spriggs, F., 2014. Matrix effect in ligand-binding assay: the importance of evaluating emerging technologies. *Bioanalysis*. <https://doi.org/10.4155/bio.14.39>.
- Dalirirad, S., Steckl, A.J., 2019. Aptamer-based lateral flow assay for point of care cortisol detection in sweat. *Sensor. Actuator. B Chem.* 283, 79–86. <https://doi.org/10.1016/j.snb.2018.11.161>.
- Edwards, K.A., Korff, R., Baeumner, A.J., 2017. Liposome-enhanced lateral-flow assays for clinical analyses. In: *Methods in Molecular Biology*. Humana Press Inc., pp. 407–434. [https://doi.org/10.1007/978-1-4939-6848-0\\_25](https://doi.org/10.1007/978-1-4939-6848-0_25).
- Fu, E., Liang, T., Houghtaling, J., Ramachandran, S., Ramsey, S.A., Lutz, B., Yager, P., 2011. Enhanced sensitivity of lateral flow tests using a two-dimensional paper network format. *Anal. Chem.* 83, 7941–7946. <https://doi.org/10.1021/ac201950g>.
- García-González, E., Aramendía, M., Álvarez-Ballano, D., Trincado, P., Rello, L., 2016. Serum sample containing endogenous antibodies interfering with multiple hormone immunoassays. Laboratory strategies to detect interference. *Pract. Lab. Med.* 4, 1–10. <https://doi.org/10.1016/j.plabm.2015.11.001>.
- Gasperino, D., Baughman, T., Hsieh, H.V., Bell, D., Weigl, B.H., 2018. Improving lateral flow assay performance using computational modeling. *Annu. Rev. Anal. Chem.* 11, 219–244. <https://doi.org/10.1146/annurev-anchem-061417-125737>.
- Gong, X., Cai, J., Zhang, B., Zhao, Q., Piao, J., Peng, W., Gao, W., Zhou, D., Zhao, M., Chang, J., 2017. A review of fluorescent signal-based lateral flow immunochromatographic strips. *J. Mater. Chem. B*. <https://doi.org/10.1039/c7tb01049d>.
- Grant, B.D., Anderson, C.E., Williford, J.R., Alonzo, L.F., Glukhova, V.A., Boyle, D.S., Weigl, B.H., Nichols, K.P., 2020. SARS-CoV-2 coronavirus nucleocapsid antigen-detecting half-strip lateral flow assay toward the development of point of care tests using commercially available reagents. *Anal. Chem.* 92, 11305–11309. <https://doi.org/10.1021/acs.analchem.0c01975>.
- Jiang, F., Hsieh, Y. Lo, 2014. Super water absorbing and shape memory nanocellulose aerogels from TEMPO-oxidized cellulose nanofibrils via cyclic freezing-thawing. *J. Mater. Chem.* 2, 350–359. <https://doi.org/10.1039/c3ta13629a>.
- Johnson, N., Ebersole, J., Kryscio, R., Danaher, R., Dawson, D., Al-Sabbagh, M., Miller, C., 2016. Rapid assessment of salivary MMP-8 and periodontal disease using lateral flow immunoassay. *Oral Dis.* 22, 681–687. <https://doi.org/10.1111/odi.12521>.
- Kasetsirikul, S., Shiddiky, M.J.A., Nguyen, N.T., 2020. Challenges and perspectives in the development of paper-based lateral flow assays. *Microfluid. Nanofluidics*. <https://doi.org/10.1007/s10404-020-2321-z>.
- Katis, I.N., He, P.J.W., Eason, R.W., Sones, C.L., 2018. Improved sensitivity and limit-of-detection of lateral flow devices using spatial constrictions of the flow-path. *Biosens. Bioelectron.* 113, 95–100. <https://doi.org/10.1016/j.bios.2018.05.001>.
- Lavoine, N., Bergström, L., 2017. Nanocellulose-based foams and aerogels: processing, properties, and applications. *J. Mater. Chem.* <https://doi.org/10.1039/c7ta02807e>.
- Levinson, S.S., Miller, J.J., 2002. Towards a better understanding of heterophile (and the like) antibody interference with modern immunoassays. *Clin. Chim. Acta*. [https://doi.org/10.1016/S0009-8981\(02\)00275-9](https://doi.org/10.1016/S0009-8981(02)00275-9).
- Li, Z., Yi, Y., Luo, X., Xiong, N., Liu, Y., Li, S., Sun, R., Wang, Y., Hu, B., Chen, W., Zhang, Y., Wang, J., Huang, B., Lin, Y., Yang, J., Cai, W., Wang, X., Cheng, J., Chen, Z., Sun, K., Pan, W., Zhan, Z., Chen, L., Ye, F., 2020. Development and clinical application of a rapid IgM-IgG combined antibody test for SARS-CoV-2 infection diagnosis. *J. Med. Virol. jmv.* 25727 <https://doi.org/10.1002/jmv.25727>.
- Mahmoudi, T., de la Guardia, M., Shirdel, B., Mokhtarzadeh, A., Baradaran, B., 2019. Recent advancements in structural improvements of lateral flow assays towards point-of-care testing. *TrAC Trends Anal. Chem. (Reference Ed.)*. <https://doi.org/10.1016/j.trac.2019.04.016>.

- Miller, J.N., Miller, J.C., 2010. *Statistics and Chemometrics for Analytical Chemistry*, Sixth. Prentice Hall, p. 123. <https://doi.org/10.1198/tech.2004.s248>.
- Mohd Hanafiah, K., Arifin, N., Bustami, Y., Noordin, R., Garcia, M., Anderson, D., 2017. Development of multiplexed infectious disease lateral flow assays: challenges and opportunities. *Diagnostics* 7, 51. <https://doi.org/10.3390/diagnostics7030051>.
- LP) (3825-1AD-6) [WWW Document], n.d. URL <https://www.mabtech.com/products/mouse-igg-elisa-development-kit-alp-3825-1ad> (accessed 11.22.20).
- Moyano, A., Serrano-Pertierra, E., Salvador, M., Martínez-García, J.C., Rivas, M., Blanco-López, M.C., 2020. Magnetic lateral flow immunoassays. *Diagnostics*. <https://doi.org/10.3390/diagnostics10050288>.
- Ng, K., Gao, B., Yong, K.W., Li, Y., Shi, M., Zhao, X., Li, Z., Zhang, X.H., Pingguan-Murphy, B., Yang, H., Xu, F., 2017. Paper-based cell culture platform and its emerging biomedical applications. *Mater. Today* 20, 32–44. <https://doi.org/10.1016/j.mattod.2016.07.001>.
- Parolo, C., Medina-Sánchez, M., De La Escosura-Muñiz, A., Merkoçi, A., 2013. Simple paper architecture modifications lead to enhanced sensitivity in nanoparticle based lateral flow immunoassays. *Lab Chip* 13, 386–390. <https://doi.org/10.1039/c2lc41144j>.
- Qiu, W., Xu, H., Takalkar, S., Gurung, A.S., Liu, B., Zheng, Y., Guo, Z., Baloda, M., Baryeh, K., Liu, G., 2015. Carbon nanotube-based lateral flow biosensor for sensitive and rapid detection of DNA sequence. *Biosens. Bioelectron.* 64, 367–372. <https://doi.org/10.1016/j.bios.2014.09.028>.
- Qu, H., Zhang, Y., Qu, B., Kong, H., Qin, G., Liu, S., Cheng, J., Wang, Q., Zhao, Y., 2016. Rapid lateral-flow immunoassay for the quantum dot-based detection of puerarin. *Biosens. Bioelectron.* 81, 358–362. <https://doi.org/10.1016/j.bios.2016.03.008>.
- Rivas, L., Medina-Sánchez, M., De La Escosura-Muñiz, A., Merkoçi, A., 2014. Improving sensitivity of gold nanoparticle-based lateral flow assays by using wax-printed pillars as delay barriers of microfluidics. *Lab Chip* 14, 4406–4414. <https://doi.org/10.1039/c4lc00972j>.
- Rosenberg-Hasson, Y., Hansmann, L., Liedtke, M., Herschmann, I., Maecker, H.T., 2014. Effects of serum and plasma matrices on multiplex immunoassays. *Immunol. Res.* 58, 224–233. <https://doi.org/10.1007/s12026-014-8491-6>.
- Saito, T., Kimura, S., Nishiyama, Y., Isogai, A., 2007. Cellulose nanofibers prepared by TEMPO-mediated oxidation of native cellulose. *Biomacromolecules* 8, 2485–2491. <https://doi.org/10.1021/bm0703970>.
- Schwickart, M., Vainshtein, I., Lee, R., Schneider, A., Liang, M., 2014. Interference in immunoassays to support therapeutic antibody development in preclinical and clinical studies. *Bioanalysis* 6, 1939–1951. <https://doi.org/10.4155/bio.14.127>.
- Sun, D., Liu, W., Tang, A., Guo, F., Xie, W., 2019. A new PEGDA/CNF aerogel-wet hydrogel scaffold fabricated by a two-step method. *Soft Matter* 15, 8092–8101. <https://doi.org/10.1039/c9sm00899c>.
- Sztefko, K., 2002. Interferences in immunoassay. *Clin. Biochem. Rev.* 59, 477–480. <https://doi.org/10.1016/b978-012214730-2/50008-x>.
- Tang, R., Yang, H., Gong, Y., Liu, Z., Li, X., Wen, T., Qu, Z., Zhang, S., Mei, Q., Xu, F., 2017. Improved analytical sensitivity of lateral flow assay using sponge for HBV nucleic acid detection. *Sci. Rep.* 7, 1360. <https://doi.org/10.1038/s41598-017-01558-x>.
- Tang, Y.W., Schmitz, J.E., Persing, D.H., Stratton, C.W., 2020. Laboratory diagnosis of COVID-19: current issues and challenges. *J. Clin. Microbiol.* <https://doi.org/10.1128/JCM.00512-20>.
- Tian, M., Lei, L., Xie, W., Yang, Q., Li, C.M., Liu, Y., 2019. Copper deposition-induced efficient signal amplification for ultrasensitive lateral flow immunoassay. *Sensor. Actuator. B Chem.* 282, 96–103. <https://doi.org/10.1016/j.snb.2018.11.028>.
- Wang, D., He, S., Wang, X., Yan, Y., Liu, J., Wu, S., Liu, S., Lei, Y., Chen, M., Li, L., Zhang, J., Zhang, L., Hu, X., Zheng, X., Bai, J., Zhang, Yulong, Zhang, Yitong, Song, M., Tang, Y., 2020. Rapid lateral flow immunoassay for the fluorescence detection of SARS-CoV-2 RNA. *Nat. Biomed. Eng.* 4, 1150–1158. <https://doi.org/10.1038/s41551-020-00655-z>.
- Wu, J.L., Tseng, W.P., Lin, C.H., Lee, T.F., Chung, M.Y., Huang, C.H., Chen, S.Y., Hsueh, P.R., Chen, S.C., 2020. Four point-of-care lateral flow immunoassays for diagnosis of COVID-19 and for assessing dynamics of antibody responses to SARS-CoV-2. *J. Infect.* 81, 435–442. <https://doi.org/10.1016/j.jinf.2020.06.023>.
- Zander, N.E., Dong, H., Steele, J., Grant, J.T., 2014. Metal cation cross-linked nanocellulose hydrogels as tissue engineering substrates. *ACS Appl. Mater. Interfaces* 6, 18502–18510. <https://doi.org/10.1021/am506007z>.